Computational Materials Science 110 (2015) 254–260

Contents lists available at ScienceDirect

Computational Materials Science

journal homepage: www.elsevier.com/locate/commatsci

Molecular dynamics study of creep mechanisms in nanotwinned metals

Shuyin Jiao, Yashashree Kulkarni *

Department of Mechanical Engineering, University of Houston, Houston, TX 77204, USA

ARTICLE INFO

Article history:
Received 24 April 2015
Received in revised form 7 August 2015
Accepted 10 August 2015

Keywords:
Twin boundaries
Molecular dynamics
Creep
Nanotwinned metals

ABSTRACT

Nanotwinned structures have shown great promise as optimal motifs for evading the strength–ductility trade-off. In this paper, we present a study of high temperature creep in polycrystalline nanotwinned face-centered cubic metals using molecular dynamics. The simulations reveal that the nanotwinned metals exhibit greater creep resistance with decreasing twin boundary spacing over a large range of applied stresses. The findings also indicate that the presence of twin boundaries entails higher stress for the onset of power-law creep compared to the nanocrystalline counterparts. Nanotwinned metals with very high density of twin boundaries exhibit a new creep deformation mechanism at high stresses governed by twin boundary migration. This is in contrast to nanocrystalline and nanotwinned metals with larger twin spacing, which exhibit a more conventional transition from grain boundary diffusion and sliding to dislocation nucleation.

1. Introduction

There is compelling evidence for the critical role of twin boundaries (TBs) in imparting the extraordinary combination of strength and ductility to nanotwinned metals [1,2]. This is in stark contrast to nanocrystalline materials, which exhibit a loss of ductility, and grain stability with decreasing grain size, thereby dampening the initial enthusiasm generated by their very high yield strength (see [3] for review). It is now well-documented that the twin boundaries strengthen by serving as effective barriers for arresting dislocation motion while simultaneously enhance ductility by absorbing dislocations onto the twin planes and accommodating plasticity. With the emerging potential of nanotwinned structures as optimal motifs for the design of high strength high ductility materials, the prospect of their creep response is of vital concern, one that would determine their true practical utility for structural applications. Although creep mechanisms in nanocrystalline materials have been investigated extensively through experiments and analytically, the topic has been relatively unaddressed in the context of nanotwinned metals, which is the focus of the present study.

The deformation mechanisms associated with creep in conventional polycrystalline metals at different ranges of applied stresses, temperatures and grain sizes are well-described by the unified Bird–Dorn–Mukherjee relation [4] given by

$$\dot{\epsilon} = \frac{AD_0Gb}{k_BT}\left(\frac{b}{d}\right)^p\left(\frac{\sigma}{G}\right)^n \exp\left(-\frac{\Delta Q}{k_BT}\right) \quad (1)$$

where $\dot{\epsilon}$ is the strain rate, A is a dimensionless constant, D_0 is a frequency factor, G is the shear modulus, b is the magnitude of the Burgers vector, k_B is Boltzmann's constant, T is the absolute temperature, d is the grain size, p is the inverse grain size exponent, σ is the applied stress, n is the stress exponent, and ΔQ is the activation energy for a particular mechanism. The Nabarro–Herring creep mechanism [5,6] that involves vacancy flow through the lattice is characterized by a $1/d^2$ dependence on the grain size, whereas Coble creep [7] that involves vacancy diffusion along the grain boundaries, exhibits a $1/d^3$ dependence. Both these mechanisms are characterized by a linear dependence on the applied stress ($n \sim 1$). Furthermore, it is well-accepted that grain boundary sliding is necessary to accommodate this diffusional transport in order to maintain compatibility of the adjoining grains and hence occurs simultaneously with diffusional creep [8]. Although at low stresses, the diffusion is rate limiting, some studies have shown analytically that at intermediate stresses, the strain rate is controlled by grain boundary sliding which is manifested in a stress exponent $n \sim 2$ [9]. $n > 4$ indicates the onset of power-law creep and is associated with dislocation-climb mediated mechanisms that become dominant at higher stresses [10].

A number of experimental studies have been carried out on creep of nanocrystalline metals at low and moderate homologous temperatures (*viz.* $T/T_m < 0.7$, T_m is the melting point) and have demonstrated various atomistic mechanisms [11–16]. Several

* Corresponding author.
E-mail address: ykulkarni@uh.edu (Y. Kulkarni).

http://dx.doi.org/10.1016/j.commatsci.2015.08.017
0927-0256/

molecular dynamics studies have also been performed to elucidate the atomistic mechanisms underpinning the creep response of nanocrystalline metals at elevated temperatures [17–19]. Creep mechanisms including grain boundary diffusion, grain boundary sliding, and dislocation nucleation have been identified under different levels of applied stress as intra-granular dislocation activity, especially dislocation climb, is severely limited by the small grain sizes. A few studies on nanotwinned metals have reported that nanotwinned Cu and Ag are much more structurally stable and retain their hardness than their nanocrystalline counterparts during microindentation creep tests and cyclic loading at room temperature [20,21]. Sanders et al. [14] have also noted the presence of a high density of twin boundaries in their as-prepared nanocrystalline Cu samples, and they believed these twins and low angle grain boundaries to play a role in the low strain rates observed in their creep tests. In the present study, molecular dynamics (MD) simulations of creep in polycrystalline nanotwinned Cu have been performed over a wide range of applied stresses to elucidate the role of coherent twin boundaries in governing the rate-controlling creep mechanisms. We emphasize that all MD simulations are inherently limited by high strain rates (of the order of 10^8 s^{-1}) and very short time scales (of the order of a few nanoseconds) that are accessible to these conventional atomistic methods. To partially circumvent this limitation, our simulations have been performed at high homologous temperatures at which the GB-mediated creep mechanisms are identifiable on the time scale of MD, and previous simulation results have shown agreement with phenomenological models and experimental data [22].

2. Simulation method

Simulations were performed on three-dimensional nanocrystalline (NC) and nanotwinned (NT) Cu specimens containing 16 randomly oriented grains in body-centered cubic distribution created by Voronoi construction [23]. The NC specimen had an overall size of about 21.8 nm × 21.8 nm × 21.8 nm consisting of 836,450 atoms. The NT specimen had an overall size of about 20.6 nm × 21.4 nm × 20.2 nm consisting of 712,335 atoms. The shape and size of the grains were kept uniform in order to avoid grain growth at the high temperatures considered in this study [17]. The grain size in NC samples was about 10.8 nm (Fig. 1(a)). Four NT samples were constructed with a twin boundary (TB) spacing of 0.6 nm, 1.2 nm, 2.5 nm, and 5 nm and a grain size of 10.3 nm. Fig. 1(b) shows the relaxed configuration of nanotwinned Cu with twin lamella thickness of 0.6 nm. Periodic boundary conditions were applied in the x, y, and z directions. Inter-atomic interactions were modeled using the embedded atom method (EAM) potential for Cu developed by Mishin et al. [24]. The samples were first equilibrated at a given temperature using the NPT ensemble for 200 ps. In order to investigate the creep response of both NC and NT samples, a constant stress was applied along the x direction for another 200 ps, while maintaining the other two directions stress-free and the resulting evolution of the strain was obtained. Creep was studied at different levels of uniaxial stress ranging from 0.05 GPa to 3.5 GPa and different temperatures, specifically, 720 K, 960 K, and 1080 K which correspond to 0.5, 0.7, and 0.8 homologous temperatures respectively. All simulations were performed using LAMMPS [25], and the atomistic structures were visualized based on common neighbor analysis using OVITO [27].

3. Results and discussion

Fig. 2(a) shows the evolution of strain with time for NC Cu and NT Cu with twin spacing of 0.6 nm subjected to different levels of stress at 960 K. All the curves exhibit a short elastic regime for the first few picoseconds, and then enter the creep stage as indicated by the change in slope. As our focus is on the analysis of steady-state creep, the creep curves only show the first two stages of creep. Therefore, for applied stress lower than 1 GPa, the simulations end at 200 ps, whereas for applied stresses above 1 GPa, the simulations are terminated at much earlier times, consistent with the simulations of Wang et al. [19] on NC Cu. As expected, all specimen exhibit larger deformation with increase in the applied stress. At all stress levels considered here, the NT specimen shows a lower creep rate when compared to its NC counterpart. Moreover, the difference in their strain curves increases steadily with the increase in the applied stress until 1 GPa. Fig. 2(b) shows the creep results for the same NT and NC specimen at 0.6 GPa under varying temperatures. All specimen exhibit increasing strain rate with increasing temperatures as expected. Comparing the response of NT and NC specimens, we observe similar trends as in Fig. 2(a) with the NT specimen exhibiting lower deformation and strain rate compared to the NC specimen at all temperatures. Fig. 2(c) shows the strain versus time plots for NT samples with different twin spacings at an applied stress of 0.5 GPa. Fig. 2(d) shows the variation of the creep rate as a function of the TB spacing at an applied stress of 1 GPa. The results reveal that the creep resistance of NT metals improves with decreasing twin spacing in comparison to the NC metals of the same grain size.

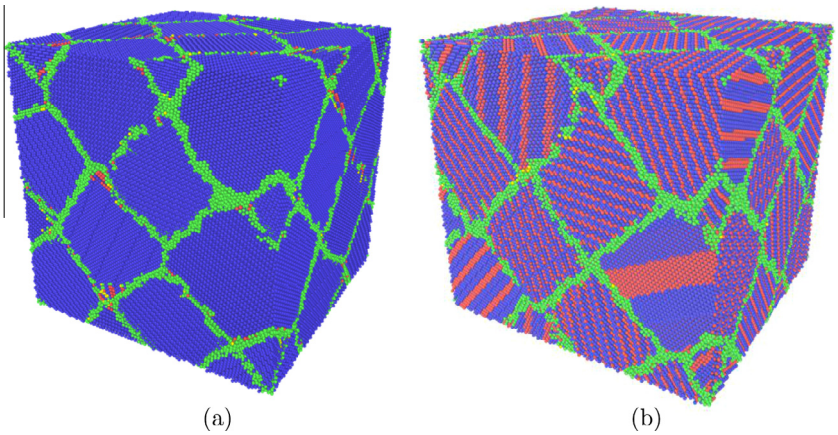

Fig. 1. Simulation specimen after thermal equilibration visualized by common neighbor analysis [26] (Blue: FCC, Red: HCP, Yellow: BCC, Green: Others) using Ovito [27]: (a) nanocrystalline (NC) Cu, (b) nanotwinned (NT) Cu with twin boundary (TB) spacing of 0.6 nm. (For interpretation of the references to color in this figure legend, the reader is referred to the web version of this article.)

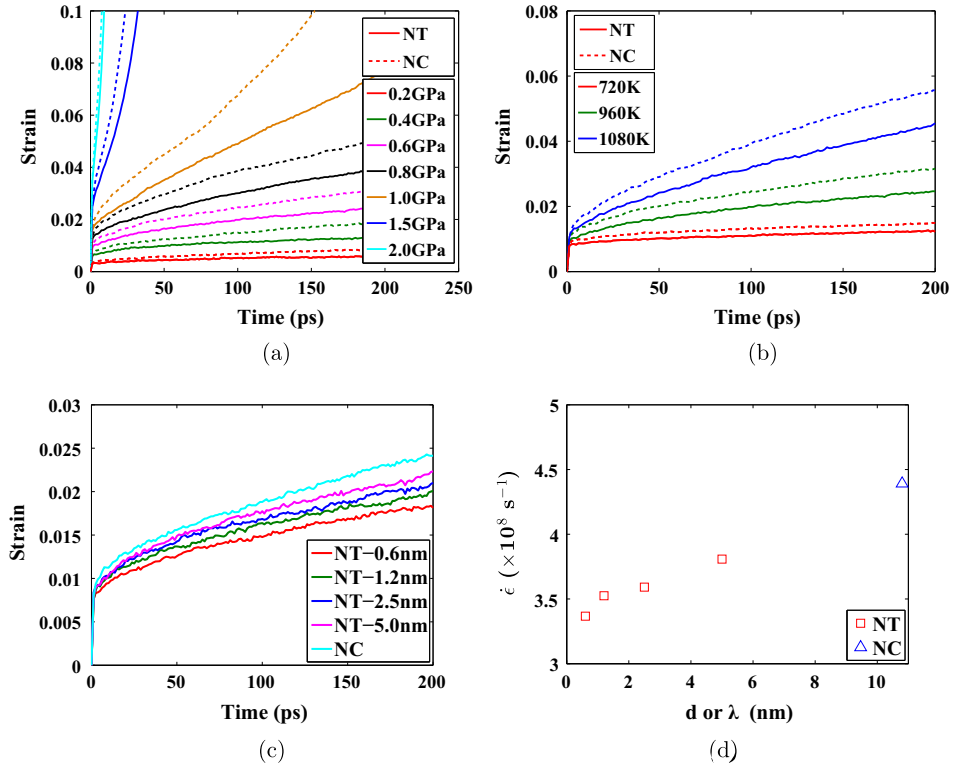

Fig. 2. (a) Creep curves for NC Cu and NT Cu with TB spacing of 0.6 nm at 960 K under different applied stresses; (b) creep curves for NC Cu and NT Cu with TB spacing of 0.6 nm under 0.6 GPa stress at different temperatures; (c) creep curves for NC Cu and NT Cu with different TB spacings under 0.5 GPa of applied stress at 960 K; and (d) variation of the creep rate versus TB spacing at applied stress of 1 GPa at 960 K. In (a) and (b), the solid lines denote NT Cu and dashed lines denote NC Cu.

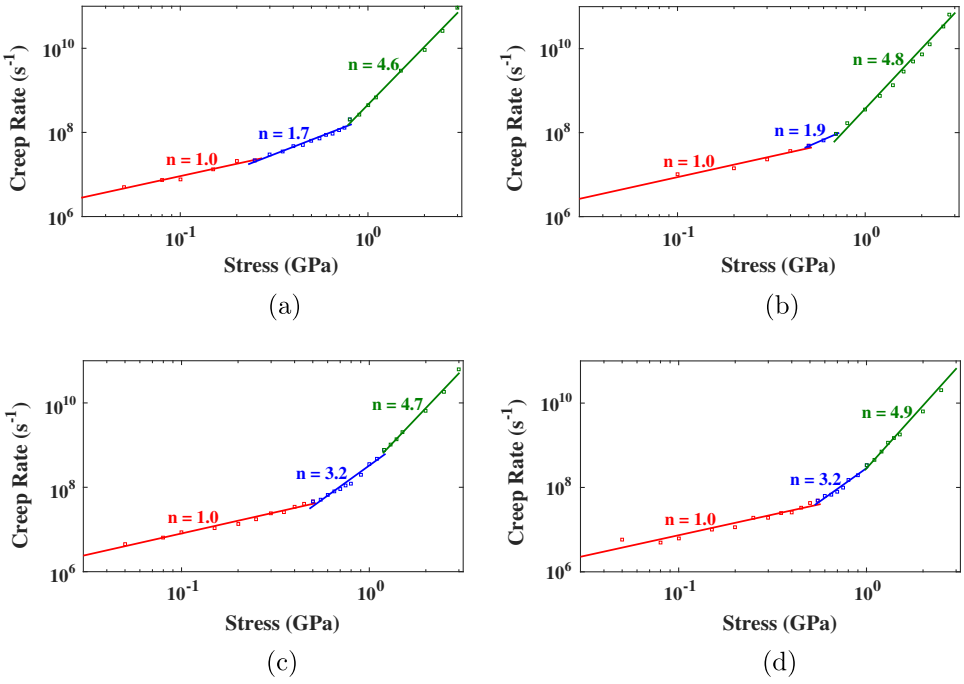

Fig. 3. Log–log plots for steady-state creep rate versus applied stress for different specimen: (a) NC Cu; (b) NT Cu with TB spacing of 2.5 nm; (c) NT Cu with TB spacing of 1.2 nm, and (d) NT Cu with TB spacing of 0.6 nm. All simulations were performed at 960 K.

According to the Bird–Dorn–Mukherjee equation (Eq. (1)), the strain rate $\dot{\epsilon}$ follows a power-law relationship with stress, which may be expressed as $\dot{\epsilon} \propto \sigma^n$. Therefore, the stress exponent n is given by $n = \partial \log \dot{\epsilon} / \partial \log \sigma$, which is simply the slope of the strain rate versus stress curve on a log–log plot. Fig. 3 shows the variation of the creep rate with stress for different specimen. The value of n for different ranges of stress is estimated as follows. The linear regime (red line) is determined by the best fit to n closest to 1.

The regime for $n > 4$ (green line) is determined by examining the atomistic structures and noting the onset of dislocation nucleation. The slope of the intermediate regime (blue line) is estimated by fitting a straight line through the remaining data points. The stress exponent is an important parameter for identifying different creep mechanisms. In their atomistic study, Wang et al. [19] have shown that there is a transition in the creep mechanism in NC Cu from GB diffusion and sliding to dislocation nucleation with increasing applied stress. This transition is also reflected in the different values of n for different stress ranges obtained from their molecular dynamics simulations. As shown in Fig. 3(a), our results for n for NC specimen of grain size of about 10.8 nm are in close agreement with those presented by Wang et al. [19]. At low applied stress range from 50 MPa to 250 MPa, $n \approx 1$, and hence the corresponding creep mechanism is expected to be diffusional creep. Owing to the very small grain size, and consequently, very high density of GBs, we expect the mechanism to be Cobble creep. To confirm this from atomistic structures, we follow the method proposed by Yamakov et al. [17] to visualize diffusion. To this end, we use markers of alternating colors to identify straight bands of atoms in a given cross-section of the undeformed specimen (Fig. 4(a)). As shown in Fig. 4(b), after creep deformation, the markers remain straight within the grains but are distorted considerably along GBs, indicating diffusion along GBs. At moderate applied stress range between 250 MPa and 800 MPa, where $n \approx 2$, creep is believed to be dominated by grain boundary sliding based on prior studies [19,9]. Fig. 4(c) identifies GB sliding at an applied stress of 0.6 GPa based on another method discussed by Yamakov et al. [17]. The intersecting markers (shown by black lines of atoms) are initially perpendicular to each other but distortions at the intersections after deformation (shown in circles) indicate sliding of the grains along GBs. Again, as noted earlier, we believe that diffusion and sliding should occur concurrently to accommodate each other in both cases ($n \approx 1$ and $n \approx 2$). Finally, at high applied stress above 800 MPa, where $n \approx 4.6$, or rather $n > 4$, we observe that dislocation nucleation becomes the dominant deformation mechanism. Atomistic structures of NC Cu in Fig. 5(a–c) illustrate dislocations nucleating from grain boundaries during steady-state creep when the stress is above 800 MPa. The density of nucleated dislocations is observed to increase with the applied stress. Fig. 5(b) shows only a few stacking faults at 200 ps when the applied stress is about 0.8 GPa which is about the stress value when the slope of the creep curve changes from 2 to larger than 4 (Fig. 3(a)). In Fig. 5 (c), however, we see more intragranular stacking faults at just 20 ps when the applied stress is about 1.5 GPa. Based on Fig. 4 (d), we observe that some GB sliding may also occur in addition to dislocation activity in the $n > 4$ region. This is consistent with the MD simulations reported by Wang et al. [19]. It is important to bear in mind that although our stress exponent in the high stress range is consistent with power-law creep ($n > 4$), the mechanisms observed are very distinct. While MD simulations show the mechanism to be dislocation nucleation, the power-law creep is understood to arise primarily from dislocation glide-climb. However, due to extremely high strain rates, dislocation climb cannot be observed in MD simulations and dislocation nucleation is the dominant deformation. Hence, it is difficult to say, purely from

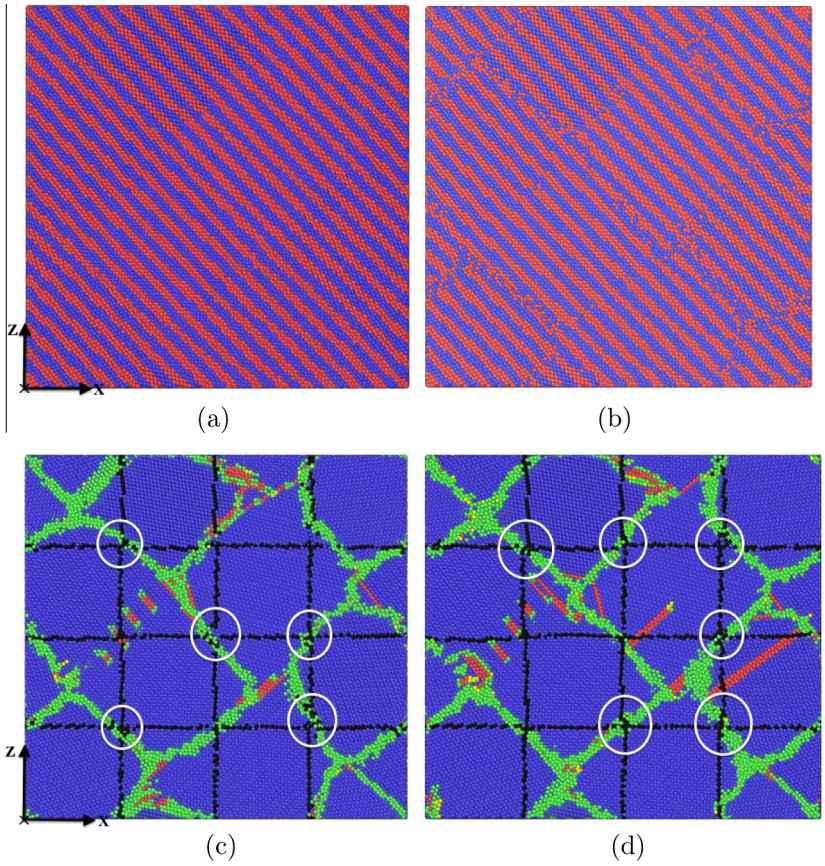

Fig. 4. Cross-sectional snapshots of NC Cu during creep at 960 K: (a) after thermal equilibration; (b) at 0.2 GPa stress after 200 ps; (c) at 0.6 GPa stress after 200 ps; (d) at 1.1 GPa stress after 50 ps. In (a) and (b), the atoms are marked as straight bands of alternating red and blue. The distortions along GBs in (b) indicate GB diffusion during creep. In (c) and (d), the atoms are marked in the form of intersecting black lines that are perpendicular to each other in the undeformed configuration (not shown). Distortions at their intersections (marked by circles) indicate GB sliding [17]. (For interpretation of the references to color in this figure legend, the reader is referred to the web version of this article.)

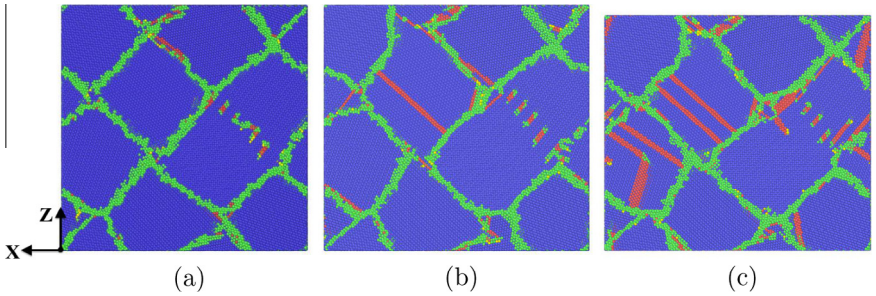

Fig. 5. Cross-sectional snapshots of NC Cu during creep at 960 K: (a) after thermal equilibration; (b) after 200 ps at 0.8 GPa stress; (c) after 20 ps at 1.5 GPa applied stress. The atomistic structures are visualized using common neighbor analysis (Blue: FCC, Red: HCP, Yellow: BCC, Green: Others). (For interpretation of the references to color in this figure legend, the reader is referred to the web version of this article.)

MD simulations, whether dislocation nucleation can be identified as a creep mechanism at nanoscale grain sizes. Experimental studies and multi-scaling modeling are needed to provide further insights.

Fig. 3(b) shows the plot for the creep rate versus stress for NT Cu with TB spacing of 2.5 nm. We find that the variation in n is similar to that for NC Cu (Fig. 3(a)) with the deformation mechanism transitioning from diffusional creep at lower stresses to dislocation nucleation from GBs at higher stresses. Fig. 3(c) and (d) show the plots for the creep rate versus stress for NT Cu with TB spacing of 1.2 nm and 0.6 nm respectively. Comparing with Fig. 3(a), we note two striking differences. First, the initial linear regime extends over a larger range of stresses. In the case of NT Cu with 0.6 nm TB spacing, the diffusional creep is the dominant mechanism up to 500 MPa compared to about 250 MPa in the case of NC Cu. This indicates that the CTBs entail a higher applied stress for the onset of power-law creep and consequently lead to lower creep rate in this stress range. Fig. 6(a) shows diffusion occurring primarily along GBs at a stress of 0.2 GPa. It also indicates that diffusion does not occur along TBs as the markers remain undistorted with the grains containing TBs. Second, there is no regime corresponding to $n \approx 2$ unlike NC Cu. Instead, we find $n \approx 3$ for intermediate stresses before transitioning to $n > 4$ for creep mediated by dislocation nucleation. What is the deformation mechanism that leads to a different stress exponent for intermediate stresses? To address this question, we examine the evolution of the atomistic structures of our NT specimen with the smallest TB spacing of 0.6 nm. As shown in Fig. 7, we observe several incidents of TB migration when the applied stress is in the range of 500–1000 MPa. In fact, the TB migration becomes more profuse with increasing stress. This observed normal motion of the TBs is a result of partial dislocations nucleating from the TB–GB junctions and gliding along the twin plane. Twin migration has also been observed as a plasticity mechanism in prior molecular dynamics studies of nanocrystalline metals [28,29]. The study by Li et al. [29] reveals a transition in mechanism from stacking faults intersecting with TBs to TB migration when the twin spacing is reduced. In particular, their simulation of NT Cu with a grain size of 10 nm and TB spacing of 0.6 nm shows that TB migration leads to softening of the specimen owing to the high density of TB–GB junctions. Interestingly, we do not see considerable softening even with 0.6 nm twin lamellar thickness, possibly because our grains are more uniform in shape and size (to avoid grain growth) compared to the specimens used by Li et al. [29]. In fact, we observe that the specimen with the smallest possible TB spacing exhibits the largest creep resistance. We further note that some GB sliding may occur in conjunction with TB migration at these intermediate stresses, although the latter is the dominant creep mechanism resulting in $n \approx 3$. This is evident from Fig. 6(b) which shows some GB-mediated diffusion and sliding in addition to TB migration. Finally, for the $n > 4$ region, we observe considerable dislocation activity. In contrast to NC Cu which shows intragranular stacking fault ribbons emanating from GBs, NT Cu exhibits stacking faults mostly nucleating parallel to the TBs due to the high density of pre-existing TBs. This is consistent with the simulations of Li et al. [29]. Stacking faults intersecting with TBs are observed only at later stages of deformation.

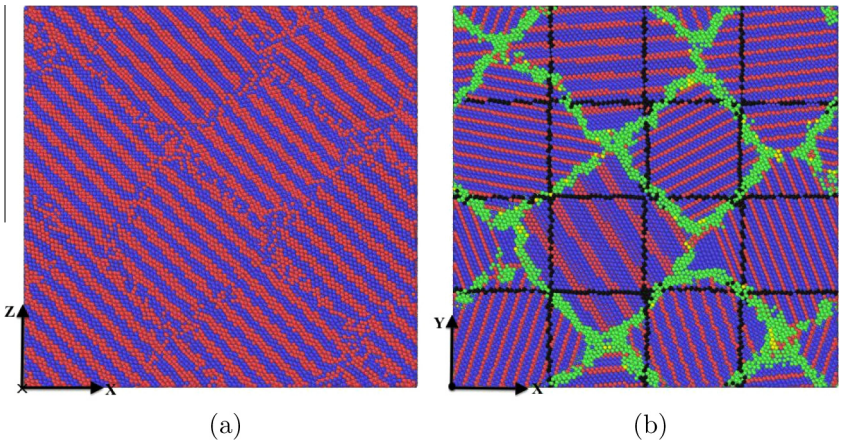

Fig. 6. Cross-sectional snapshots of NT Cu with twin spacing of 0.6 nm during creep at 960 K: (a) at 0.2 GPa stress after 200 ps; (b) at 0.7 GPa stress after 200 ps. In (a) the atoms are marked as straight bands of alternating red and blue. The distortions along GBs indicate GB diffusion. In (b) the intersecting markers are perpendicular to each other in the undeformed configuration (not shown). Distortions at their intersections indicate GB sliding. (For interpretation of the references to color in this figure legend, the reader is referred to the web version of this article.)

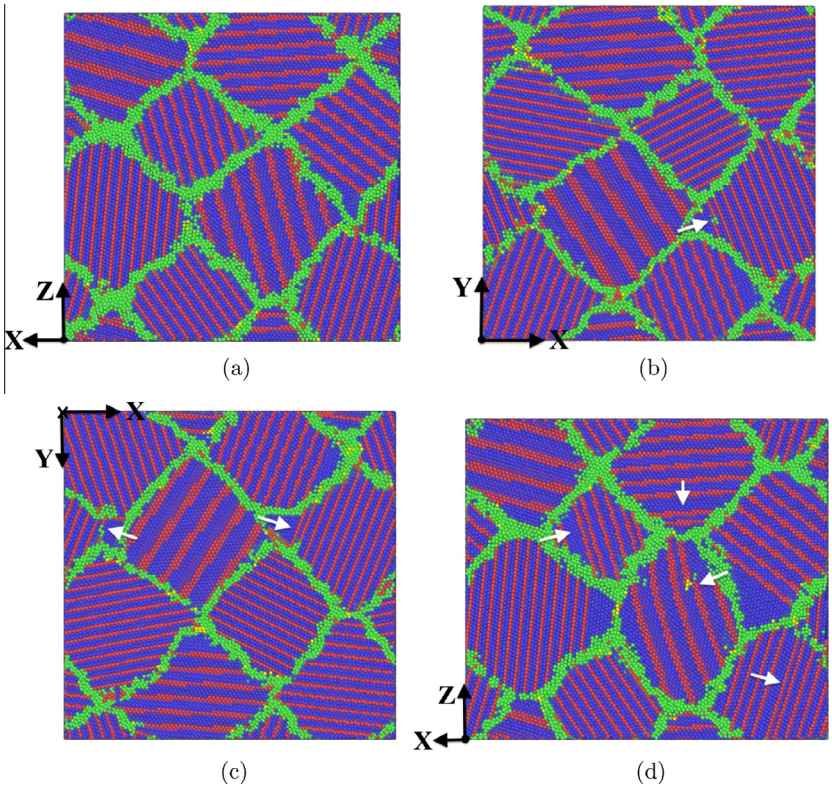

Fig. 7. Cross-sectional snapshots of NT Cu with TB spacing of 0.6 nm during creep at 960 K: (a) after thermal equilibration; (b) At 0.5 GPa stress after 200 ps; (c) At 0.7 GPa stress after 200 ps; (d) At 1 GPa stress after 200 ps.

Comparing Fig. 3(a) and (d), we note that there is an intermediate stress range of about 0.55–0.8 GPa, when $n \approx 2$ for NC Cu and $n \approx 3$ for NT Cu with 0.6 nm TB spacing. A simplistic interpretation of these results using the power-law for creep may lead us to expect that the steady state creep rate and the strain deformation for NT Cu should be greater than that for NC Cu in this overlapping stress range. However, a closer look at the data presented in Fig. 3 reveals that the creep rate for NC Cu is consistently higher than that for NT Cu. For instance, we consider the applied stress of 0.6 GPa which lies in the $n \approx 2$ region for NC Cu and the $n \approx 3$ region for NT Cu with 0.6 nm TB spacing. The $\dot{\epsilon}$ for the former is 8.6×10^7 s^{-1} which is larger than the $\dot{\epsilon}$ for the latter which is 6.2×10^7 s^{-1}. Furthermore, the strain versus time results (Fig. 2(a)) also indicate that the strain for NT Cu is always lower than NC Cu for all stresses simulated. This implies that the power-law $\dot{\epsilon} \propto \sigma^n$ is a mere indicator of the trend followed by the creep rate as a function of the applied stress; the precise value of the strain rate can depend on other factors such as the parameters that go into the proportionality coefficient. Another possible reason for the low creep rate of NT Cu despite $n \approx 3$ is that the linear regime in the case of NT Cu with 0.6 nm TB spacing extends over a larger stress range (up to 0.55 GPa) thus keeping the creep rate lower when the $n \approx 3$ region begins. Compared to this, in the case of NC Cu, the linear regime transitions to the $n \approx 2$ region sooner (at about 0.25 GPa) which leads to a faster increase in creep rate.

The activation volume, which is defined as $\Omega = \sqrt{3}k_B T \partial ln\dot{\epsilon}/\partial\sigma$, is another important parameter for identify the rate-controlling deformation mechanisms of metals and alloys and is estimated from the slope of the $\ln\dot{\epsilon}$ versus stress curve [30,31]. In microcrystalline Cu, when dislocation motion dominates plasticity, the activation volume is usually about $1000b^3$, where b is the Burgers vector, making it a fairly rate-insensitive process [32–34]. With the decrease in the grain size down to the nanometer length scale, dislocation motion is significantly suppressed by the higher fraction of grain boundaries in the system and GB-mediated processes become the dominant mechanisms [35]. This transition results in activation volumes in nanocrystalline metals almost one to two orders of magnitude smaller depending on the grain size, and a concomitant increase in strain rate sensitivity [36,37]. Fig. 8 compares the curves for $\ln\dot{\epsilon}$ versus applied stress for NC Cu and NT Cu with twin spacing of 0.6 nm obtained from our simulations. For NC Cu of a grain size of about 10 nm, the maximum activation volume is obtained to be about $9b^3$. The result is in excellent agreement with the simulations of Wang et al. [19] which yield a value of $10b^3$, and the analytical work of Asaro and Suresh [38] which predicts the range to be $3–10b^3$ for NC metals. It is interesting to note that NT Cu shows very similar variation of the $\ln\dot{\epsilon}$ versus stress

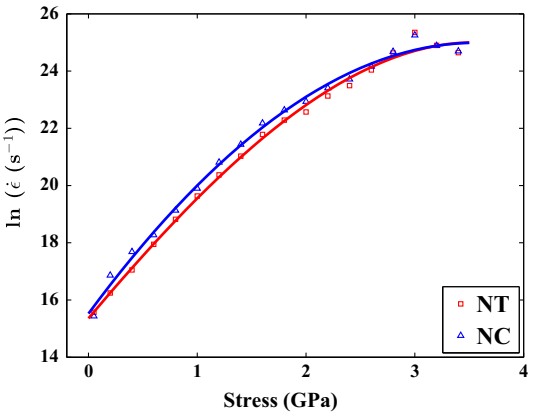

Fig. 8. Variation of the $\ln\dot{\epsilon}$ versus applied stress in NC Cu and NT Cu with 0.6 nm TB spacing at 960 K.

despite the extremely small TB spacing and the transition in creep mechanism to TB migration. We speculate that the activation volume is affected primarily by the already restrictive grain size of about 10 nm and hence reflects ostensibly no difference due to the presence of TBs in our simulations.

4. Conclusion

Our molecular dynamics study elucidates the role of twin boundaries in lowering the creep rate in nanotwinned metals with decreasing twin spacing. The nanotwinned metals exhibit improved creep response at all applied stresses and temperatures studied here in comparison to nanocrystalline metals with the same grain size. We observe TB migration as a new creep mechanism dominant at intermediate stresses in nanotwinned structures with angstrom-scale twin spacing of about 0.6 nm in a grain size of about 10 nm. This is the rate-controlling mechanism at stresses ranging from 500 MPa to 1000 MPa and leads to a stress exponent of about 3. We note that the molecular dynamics study by Li et al. [29] shows that the optimal twin spacing for maximum yield strength is dependent on the grain size. Such interplay of twin and grain size effects could also play a role in determining the rate-controlling mechanisms and the overall creep response of nanotwinned structures. Furthermore, unlike their conclusions, we do not observe any noticeable softening of the strain versus time curve for samples with high density of CTBs in our creep simulations. Hence, more creep tests on larger grain sizes spanning a range of twin lamellar thickness are needed to provide insights into the optimal twin spacing as a function of grain size in the context of creep behavior. Further studies can also shed light on the implications of TB migration as a rate-controlling creep mechanism and its interplay with GB sliding as indicated by the change in the stress exponent. In this regard, it is also interesting to examine how these results for creep mechanisms, specifically the role of TB migration, would extend to different fcc metals. Our previous work has investigated the deformation mechanisms governing the strength and stability of nanotwinned structures in various fcc metals [39,40]. Based on these studies, we speculate that the creep response of Ag and Pd should be similar to Cu at equivalent homologous temperatures since the twin boundaries in these metals exhibit similar properties. Al, in turn, may show TB migration at lower stresses due to its low resistance to shear coupled normal motion, and consequently higher tendency for TB migration. A final note of caution related to the use of molecular dynamics is in order here since these conventional atomistic approaches are generally incapable of capturing the atomistic dynamics on the scale of microseconds and beyond. Consequently, our simulations, or other molecular dynamics studies for that matter, suffer from extremely high strain rates and hence are not ideally suited for studying time-dependent phenomena such as creep. In order to partially circumvent this limitation, all simulations have been performed above 0.5 homologous temperature, at which atomistic results are known to be consistent with experimental data for these metals [22]. Nevertheless, studying the transition in creep mechanisms at realistic strain rates and temperatures using novel timescaling approaches presents an exciting avenue for future work.

Acknowledgments

The authors would like to acknowledge the support of the US National Science Foundation under grant CMMI-1129041. The simulations were performed on the supercomputing facility hosted by the Research Computing Center at University of Houston.

References

[1] L. Lu, X. Chen, X. Huang, K. Lu, Science 323 (2009) 607.
[2] Y. Wei, Y. Li, L. Zhu, Y. Liu, X. Lei, G. Wang, Y. Wu, Z. Mi, J. Liu, H. Wang, H. Gao, Nat. Comm. 5 (2014) 3580.
[3] M. Dao, L. Lu, R.J. Asaro, J.T.M. De Hossan, E. Ma, Acta Mater. 55 (2007) 4041.
[4] A.K. Mukherjee, J.E. Bird, J.E. Dorn, ASM Trans. 62 (1969) 155.
[5] F.R.N. Nabarro, Proc. Conference on Strength of Solids, vol. 75, The Physical Society, London, 1948.
[6] C. Herring, J. Appl. Phys. 21 (1950) 437.
[7] R.L. Coble, J. Appl. Phys. 34 (1963) 1679.
[8] R. Balluffi, S. Allen, W.C. Carter, Kinetics of Materials, Wiley, 2005.
[9] H. Luthy, R.A. White, O.D. Sherby, Mater. Sci. Eng. 39 (1979) 211.
[10] H. Riedel, Fracture at High Temperatures, Springer-Verlag, 1987.
[11] F.A. Mohamed, Y. Li, Mater. Sci. Eng. A 298 (2001) 1.
[12] G.W. Nieman, J.R. Weertman, R.W. Siegel, J. Mater. Res. 6 (1991) 1012.
[13] D.L. Wang, Q.P. Kong, J.P. Shui, Scripta Metall. Mater. 31 (1994) 47.
[14] P.G. Sanders, M. Rittner, E. Kiedaisch, J.R. Weertman, H. Kung, Y.C. Lu, Nanostruct. Mater. 9 (1997) 433.
[15] H. Fukutomi, H. Takatori, R. Horiuchi, Trans. Jpn. Inst. Met. 23 (1982) 579.
[16] S. Gollapudi, K.V. Rajulapati, I. Charit, C.C. Koch, R.O. Scattergood, K.L. Murty, Mater. Sci. Eng. A 527 (2010) 5773.
[17] V. Yamakov, D. Wolf, S.R. Phillpot, H. Gleiter, Acta Mater. 50 (2002) 61.
[18] A.J. Haslam, V. Yamakov, D. Moldovan, D. Wolf, S.R. Phillpot, H. Gleiter, Acta Mater. 52 (2004) 1971.
[19] Y.J. Wang, A. Ishii, S. Ogata, Phys. Rev. B 84 (2011) 224102.
[20] C.J. Shute, B.D. Myers, S. Xie, S.-Y. Li, T.W. Barbee Jr., A.M. Hodge, J.R. Weertman, Acta Mater. 59 (2011) 4569.
[21] J. Bezares, S. Jiao, Y. Liu, D. Bufford, L. Lu, X. Zhang, Y. Kulkarni, R.J. Asaro, Acta Mater. 60 (2012) 4623.
[22] D. Wolf, V. Yamakov, S.R. Phillpot, A. Mukherjee, H. Gleiter, Acta Mater. 53 (2005) 1.
[23] <http://li.mit.edu/Archive/Graphics/A/utils.html>.
[24] Y. Mishin, M.J. Mehl, D.A. Papaconstantopoulos, A.F. Voter, J.D. Kress, Phys. Rev. B 63 (2001) 224106.
[25] S.J. Plimpton, J. Comp. Phys. 117 (1995) 1.
[26] J.D. Honeycutt, H.C. Andersen, J. Phys. Chem. 91 (1987) 4950.
[27] A. Stukowski, Modell. Simul. Mater. Sci. Eng. 18 (2010) 015012.
[28] A. Frøseth, H. Van Swygenhoven, P.M. Derlet, Acta Mater. 52 (2004) 2279.
[29] X. Li, Y. Wei, L. Lu, K. Lu, H. Gao, Nature 464 (2010) 877.
[30] T. Zhu, J. Li, A. Samanta, H.G. Kim, S. Suresh, PNAS 104 (2007) 3031.
[31] R.J. Asaro, Y. Kulkarni, Scripta Mater. 58 (2008) 389.
[32] P.S. Follansbee, U.F. Kocks, Acta Metall. 36 (1988) 81.
[33] R.P. Carrekar, W.R. Hibbard, Acta Metall. 1 (1953) 64.
[34] P.S. Follansbee, G. Regazzoni, U.F. Kocks, Inst. Phys. Conf. Ser. 70 (1984) 71.
[35] V. Yamakov, D. Wolf, S.R. Phillpot, A.K. Mukherjee, H. Gleiter, Nat. Mater. 3 (2004) 43.
[36] Q. Wei, S. Cheng, K.T. Ramesh, E. Ma, Mater. Sci. Eng. A 381 (2004) 71.
[37] L. Lu, R. Schwaiger, Z.W. Shan, M. Dao, K. Lu, S. Suresh, Acta Mater. 53 (2005) 2169.
[38] R.J. Asaro, S. Suresh, Acta Mater. 53 (2005) 3369.
[39] Y. Kulkarni, R.J. Asaro, Acta Mater. 57 (2009) 4835.
[40] T. Sinha, Y. Kulkarni, J. Appl. Phys. 109 (2011) 114315.